Mem. S.A.It. Suppl. Vol. 1, 199

Memorie della
Supplementi

Dynamics of collisionless self-gravitating structures

G. Murante[1], S. Bonometto[2,3],
A. Curir[1], A.V. Macció[2,3], and P. Mazzei[4,]

[1] I.N.A.F., Osservatorio Astronomico di Torino, Strada Osservatorio 20, 10025 Pino Torinese,TO (Italy) e-mail: murante@to.astro.it

[2] Department of Physics G. Occhialini, Università di Milano–Bicocca, Piazza della Scienza 3, 20126 Milano (Italy)

[3] I.N.F.N., Via Celoria 16, 20133 Milano (Italy)

[4] I.N.A.F., Osservatorio Astronomico di Padova, Vicolo dell'Osservatorio 5, 35122 PADOVA

Abstract. The dynamic of collisionless, self–gravitating structures is fundamental in the context of the hierarchical model of structure formation in Cosmology. Here we shortly describe two examples in which such dynamics can be investigated using N-Body high resolution simulations.
Firstly, we show that virialized haloes are characterised by the existence of a well–defined *boundary layer* (BL). BLs are found in high–resolution simulations of galaxy clusters, but we show that they can also be detected when the resolution is decreased. We compare the dynamical mass of haloes, evaluated using the virial theorem, with the "numerical" one, obtained by directly counting the particles inside the BLs. We find excellent agreement between these two estimates of the masses. We also apply the BL method to a galaxy–size halo, showing that, also in this case, the correct virial mass is recovered.
In our second example, an exponential stellar disk is embedded in the galaxy–sized halo. The different dynamics of the two collisionless components, star and dark matter, is analysed. Our aim is to study numerically the stability of a disk in a fully cosmological halo. We vary the disk/halo mass ratio and the redshift of the embedding. Here we report preliminary results concerning the growth of bar instability in the disk.

Key words. theory: dark matter – methods: numerical – clusters of galaxies: structure – galaxies: structure – galaxies: kinematics and dynamics

Send offprint requests to: G. Murante
Correspondence to: Strada Osservatorio 20, 10025 Pino Torinese (TO)

1. Introduction

The Cold Dark Matter (CDM) scenario has proved to be quite successful in describing

structure formation and evolution. In this scenario, the *collisionless* cold dark matter drives the gravitational collapse and the subsequent evolution of initial density fluctuations.

Therefore, it is important to understand the dynamics of self gravitating, collisionless structures. N-Body simulations have become the most commonly used tool to perform this kind of investigations. Anyway, a careful dynamical study usually requires high resolution in both mass and force. Even parallel codes running on supercomputers cannot achieve the needed resolution. For this reason, a re–simulation technique (see e.g. Katz & White, 1993; Tormen, Bouchet & White 1997), is often employed when a single object is investigated. Here we shortly describe two numerical studies in which such a technique is employed.

In the first one, we show how the virialized region of DM haloes can be precisely identified. This goal is achieved by identifying a spherical shell (a *boundary layer*) which contains the virialized region of DM haloes, while outside such equilibrium is lost. The full description of this method is given elsewhere (Macció, Murante & Bonometto, 2003).

In the second study, we use a galaxy-sized halo, formed in a cosmological simulation, as the environment of an exponential stellar disk. The two components, "stars" and DM, are both collisionless, but their dynamics is different. Using high resolution simulations we follow the evolution of the disk and its feedback on the DM halo.

In both cases, the re–simulations are performed using the following implementation of the multi–mass technique, part of the ART N-Body package (Kravtshov, Klypin & Khokhlov, 1997, thanks to A. Klypin). We first set up a realization of the initial spectrum of perturbations, so that initial conditions for our largest number of particles are generated in the simulation box. The resolution in force and mass is then lowered where needed (in the outer regions and/or for lower–resolution runs), by averaging on velocities and displacements of the smaller–mass particles.

Section 2 describes the boundary layer technique, giving a short mathematical derivation and showing some application of the obtained prescription to numerical simulations. In Section 3 we present the study of the stability of a stellar disk embedded in our galactic–sized DM halo.

2. Boundary Layers in CDM haloes

One of the problems everybody faces when dealing with N–Body cosmological simulations is the very identification of objects. Indeed, haloes are not isolated and have to be distinguished from their environment. Once the position of the halo is given, its "virialized" volume is commonly defined as the sphere surrounding a given overdensity Δ_v. This definition is based on the assumption of isolated fluctuation growth, starting from and preserving spherical symmetry (Gott & Rees 1975, Lahav et. al. 1991, Eke et al. 1996, 1998, Brian & Norman 1998).

Here we present a method to define and identify a spherical shell, a *boundary layer*, which marks the transition between an inner halo, characterised by virial equilibrium, and its outer environment in which the equilibrium is lost. In our work, the assumption of isolated growth is absent, while spherical symmetry is tested, *a posteriori*, on our simulated clusters of galaxies. In this way we find that actual clusters closely approach properties predicted under such assumptions.

2.1. How to find BL

We start from the definition of *integral* potential and kinetic energy and their *virial ratio*:

$$2T(<r) = \sum_{i \ (r_i<r)} m v_i^2 \ ,$$

$$W(<r) = -\sum_{i<j \ (r_{i,j}<r)} \frac{Gm^2}{r_{ij}} \ ,$$

$$\mathcal{R}(< r) = -\frac{2T(< r)}{W(< r)} \ . \qquad (2.1)$$

Similar quantities can be defined for r–intervals, i.e. in shells having width Δr. In this case we will have $r_i \in \Delta r$. The r dependence of W can be outlined by performing the sums in eq. (2.1). Let's define

$$\mathcal{Z}(r_i) = \sum_{j \ (r_j < r_i)} \frac{Gm^2}{r_{ij}}; \qquad (2.2)$$

then we have for the potential

$$W(< r) = -\sum_{i \ (r_i < r)} \mathcal{Z}(r_i). \qquad (2.3)$$

Note that, in eq. (2.2), when $\mathcal{Z}$ is defined for r–intervals, $r_j < r_i,\ r_i \in \Delta r$: the potential for a shell is given by particles in and inside the shell itself.

In general, a volume integral of $\rho(r)$ increases with r. Thus, we can express $\mathcal{Z}$ as: $\mathcal{Z}(r) = C(r/\bar{r})^{-w}$, where C is a normalisation constant evaluated at an arbitrary position $\bar{r}$ and $w(< 1)$ depend on r. Using this expression, we get

$$r\frac{d\mathcal{Z}}{dr}(r) = -\left[w + rw' \ln\left(\frac{r}{\bar{r}}\right)\right]\mathcal{Z}(r) \ . \quad (2.4)$$

Now suppose that there exists an interval $\Delta r = r_+ - r_-$, which satisfies the following conditions:

(i) virial equilibrium, $2T(r) + W(r) = 3\Delta(pV)$;
(ii) dynamical equilibrium, i.e. external pressure forces do not act to displace it, $\Delta(pV) = 0$;
(iii) w is constant inside it.

Using eq. (2.4) with $w' = 0$, and the expression for the *virial ratio* in Δ_r we obtain:

$$\mathcal{R} = w \qquad , \qquad \frac{d\mathcal{R}}{dr} = 0 \qquad (2.6)$$

all along the interval Δr. *Viceversa*, if the eq.s (2.6) are both fulfilled in a layer of depth Δr, such layer is at rest and in virial equilibrium. We thus define *boundary layer (BL)* a region of depth Δr satisfying eq.s (2.6). It can also be shown (Macció, Murante, Bonometto 2003) that no further materials can be in virial equilibrium by requiring that w is maximum in Δr and therefore $w' < 0$ for $r > r_+$.

2.2. Application to numerical simulations

The method described above can be used to find BLs of dark matter haloes in numerical simulations. We apply it to two sets of simulations of galaxy cluster. In the first set we have two large volume simulations (box side=$360h^{-1}$ Mpc), run with a parallel AP3M code developed by Gardini et al. (1999). They describe a tilted CDM (TCDM) model ($n = 0.8$) and a ΛCDM model ($\Omega_m = 0.35$, $\Omega_\Lambda = 0.65$); these were also used in Macciò et al. (2001; simulations A and B respectively). This set of simulations provides a significant statistics, although mass and force resolution (180^3 particles, $\sim 40\,$kpc Plummer–equivalent softening) are limited. The second set of simulations has been run to provide high–resolution clusters, using the PM ART code (Kravtshov, Klypin & Khokhlov, 1997) and/or the public parallel tree–code GADGET (Springel et. al 2001). Using the re-simulation technique described in Section 1, we resolve clusters with more than 300.000 particles within a radius of 2 h^{-1} Mpc, and a mass resolution of 1.2 $\times 10^{10}\Omega_m h^{-1} M_\odot$. We performed simulations C and D of ΛCDM ($\Omega_m = 0.3$, $\Omega_\Lambda = 0.7$) and TCDM ($n = 0.8$) models, obtaining 6 high resolution clusters for each model. One of the clusters was run with both ART and GADGET, to check that no difference in our analysis arises from the use of different N-Body codes.

To find the position of BL, in each dark matter halo, we first calculate the virial ratio $\mathcal{R}$ in successive layers; then, we select radii r_i where $\mathcal{R}$ has a minimum and (nearly) intersects w, which has a maximum in r_i. This choice ensures that eq.s 2.6 are fulfilled. Results are shown in Fig. 1 for the best and worst cases we found in the

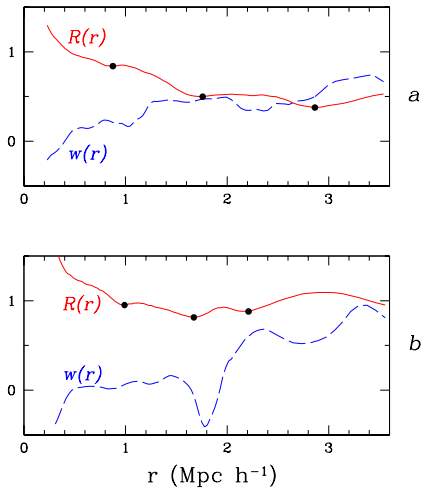

Fig. 1. The $\mathcal{R}$ and w dependence on r is shown in the best and worst cases treated at the highest resolution level, (Panels a and b, respectively). In panel a we can see a neat intersection of the two curves for a maximum of w and a minimum of $\mathcal{R}$. However, also in the case shown in Panel b, the correspondence between the maximum of w and the minimum of $\mathcal{R}$ is clear.

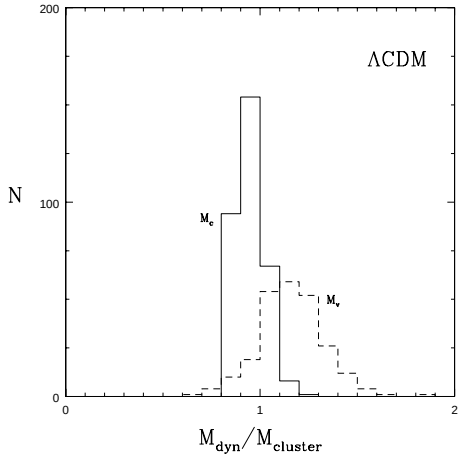

Fig. 2. The ratio between masses evaluated from particle velocities, according to the virial theorem (M_{dyn}), and summing particle masses ($M_{c,v}$) is shown for all clusters of simulation A.

simulations C and D. Even in worst case, the coincidence between a minimum of $\mathcal{R}$ and a maximum of w is neat. In simulations A and B, w is not so well traced. This it is expected, since w is obtained from differentiation and this set of simulations is characterised by a lower resolution. However, w is only used to select among minima of $\mathcal{R}$, when we have several of them: the procedure works in 97% of cases, allowing to detect a precise position for the BL.

A first, important result of our analysis is shown in Fig. 2 (here we show the result for ΛCDM model only). Once the BL for each halo is set, the halo mass M_c can easily be obtained by by summing up the masses of all the particles lying inside the BL. Correspondingly, we can also define a sphere, with radius r_v, inside which the density contrast is Δ_v; we use for the virial density contrast the approximation $\Delta_v = 18\pi^2\Omega_m^{0.45}$ (See Brian & Norman, 1998). For our ΛCDM model, $\Delta_v \approx 111$. Inside r_v we can again sum up each particle mass to obtain a halo mass M_v. We compare these values of the masses with the dynamical estimates

$$M_{dyn,\{v,c\}} = \frac{\langle v^2 \rangle_{\{v,c\}} \cdot r_{\{v,c\}}}{G}. \qquad (2.7)$$

$M_{dyn,v}$ and $M_{din,c}$ are evaluated averaging over the velocities of the particles within r_v and r_c respectively.

This comparison yields a quite reasonable coincidence between M_v and $M_{dyn,v}$ as is shown in Fig. 2 by the dashed histograms (which confirm the slight excess of $M_{dyn,v}$ *vs* M_v already noticed by previous authors). More interestingly, the agreement between $M_{dyn,c}$ and M_c, obtained on the basis of the setting of the BL (continuous line), is even better. The average value of $M_{dyn,c}/M_c$ is $\sim 0.97 \pm 0.03$. From this result, we deduce that the BL method is successful in correctly detecting the virial volumes of DM haloes. When a spherical approximation for such volumes is used, BLs give a better estimate than the commonly

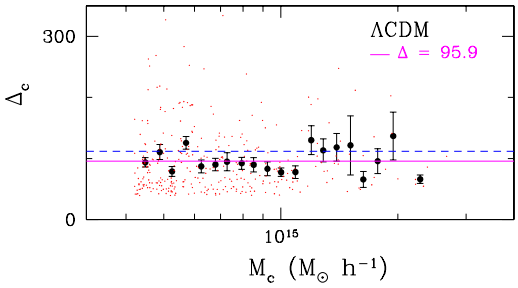

Fig. 3. The mass dependence of the density contrast is shown. Points refer to all clusters in the simulation A (ΛCDM). Heavy points give the average Δ_c for each M_c interval (constant logarithmic width). Bars are 1–σ errors of the averages. The thick horizontal line is the average value of Δ_c. The dashed line is the virial density contrast Δ_v expected for a unperturbed spherical fluctuation growth.

employed fixed density contrast approach. Results for TCDM model are similar.

We note that in numerical simulations halo shapes have various degrees of a–sphericity. Moreover, haloes are not isolated systems. Therefore, we do not necessarily expect to find any BL. Nevertheless, they are found in 97% of cases using low–resolution simulations (A and B), and in all of the high resolution clusters. The very good agreement between the estimates $M_{dyn,c}$ and M_c suggests that the spherical approximation for such volumes is acceptable. However, this point is further discussed in Macció, Murante & Bonometto (2003), where results for TCDM model are also shown.

Once the sphere confining cluster material is set, we can evaluate the corresponding density contrast Δ_c. In Fig. 3, points give Δ_c and M_c for all clusters (ΛCDM model). We notice that the spread of Δ_c values is fairly wide, thus explaining the different value of the ratios $M_{dyn,v}/M_v$, $M_{dyn,c}/M_c$. By subdividing the M_c abscissa in intervals of constant logarithmic width, we evaluate the average density contrast in each of them, to seek systematic trends with mass.

Owing to the spread of Δ_c values, their average is still subject to a significant uncertainty, shown, at the 1–σ level, in the plot. There seems to be no evidence of any peculiar trend of density contrasts with mass apart, perhaps, a modest indication of an increasing density contrast, at very high scales. It is therefore licit to consider the overall average among Δ_c's. Such average is indicated by the continuous horizontal line and compared with the "virial" density contrast Δ_v. Δ_v (dotted line) is well inside the range of the density contrasts we found; however, the average Δ_c is smaller than Δ_v by ∼25 %.

2.3. Application to galactic haloes

Our two sets of simulations are focused on the galaxy clusters mass scale, and therefore the results presented in the previous subsection concerns that mass scale. To verify the usefulness of the BL algorithm on the galaxy mass scale, we tried to detect a BL also in a halo with virial mass $M \approx 10^{11} h^{-1} M_\odot$ at redshift $z = 0$. We choosed the same DM halo used to embed the galactic stellar disk, in the numerical experiment described below.

At $z = 0$ we found a BL with radius $r_c = 0.113 h^{-1}$ Mpc, yielding a ratio $M_c/M_{dyn} = 1.0502$. The value or r_v (obtained using a fixed density contrast Δ_v) for this halo is $r_v = 0.097 h^{-1}$ Mpc. This case suggests that the BL prescription is working also on galactic mass scales. As a counter-example, we also analysed an isolated halo, characterised by a r^{-1} radial density profile, a multivariate Maxwellian distribution for the velocities, a nominal radius $R = 0.180 h^{-1}$ Mpc and the same mass as our galactic halo. The density profile is cut off at the nominal radius. This halo has been generated ad–hoc and it is *not* expected to be in virial equilibrium. The analysis *did not find any BL*, implying that (at least in this case) no "spurious" virialized volume is detected by our prescription.

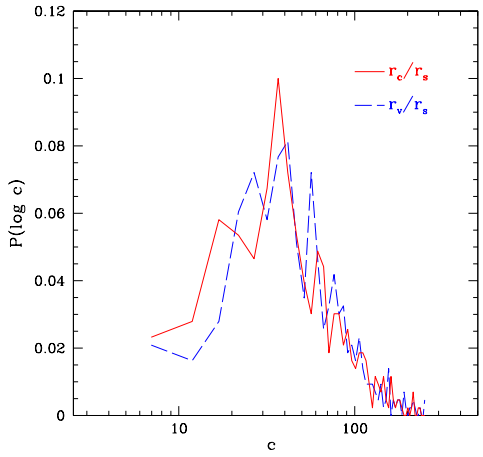

Fig. 4. Probability of having a concentration parameter c, as a function of c, for haloes lying in the mass range $1 \cdot 10^{12} - 5 \cdot 10^{12} h^{-1} M_{\odot}$, taken from the simulation described in the text. Red (solid) line refers to c_c, blue (dashed) line to c_{200}.

As a first example, we are now applying the BL method to the study of the *concentration parameter*. Such parameter can be defined as $c_{200} = r_{200}/r_s$, where r_{200} is the radius of a sphere enclosing an overdensity of 200 times the critical density of the Universe, and r_s is the scale radius of the density profile of haloes (see e.g. Navarro et al. 1996, 1997). The distribution of the concentration parameter has been studied, e.g., for haloes lying in a narrow range of masses around $10^{12} h^{-1} M_{\odot}$ (Bullock et al, 2001). However, the concentration c is not uniquely defined among different authors; both r_{200} and r_v have been used in the definition. This parameter is often used to compare theoretical predictions of the hierarchical CDM model with the data (see e.g. van den Bosch & Swaters 2001, de Blok, McGaugh & Rubin 2001). Obviously, it can be possible to measure the virial *mass* on the data, but the virial *radius* requires further hypothesis. In particular, a fixed density contrast Δ_v is often assumed to get virial radii from virial masses. But we have seen that a spread of overdensites in virialized haloes should be expected (see above, Fig. 2). Thus, we use the BL method to define the concentration parameter as $c_c = r_c/r_s$. We apply this definition to DM haloes extracted from a new set of numerical simulations, which we are currently running with the ART code. These simulations have a box size of $60h^{-1}$ Mpc, 128^3 particles, 256^3 grid points, and 7 refinement levels, giving a nominal length resolution of $2h^{-1}$ kpc (this work is being performed in collaboration with prof. A. Klypin). Here we present a preliminary result concerning the distribution of the concentration parameter for the 430 haloes detected in the mass range $1 \cdot 10^{12} - 5 \cdot 10^{12} h^{-1} M_{\odot}$ for a ΛCDM model having the same parameters as simulations C and D. To see if the *theoretical* distribution of the concentration parameter do differ using the two definitions c_c and $c_v = r_v/r_s$, in Fig. 4 we plot the two probabilities of having a given concentration parameter *vs* the concentration. A difference is easily noticed for small values of c. Further work is clearly needed to improve the statistic (i.e., the number of haloes) and to determine the statistical significance of this difference.

3. Galactic stellar disks in cosmological haloes

DM haloes are collisionless by definition. On the other hand, the same physics rules the evolution of the stellar component of galaxies, as far as the investigated scale lengths are large enough and the effect of star-star encounters can be averaged out. Indeed, N-Body simulations have commonly been used to study the birth and the growth of the bar instability in stellar disks embedded in spherical (Sellwood 1981; Athanassoula et al. 1987; Debattista, Sellwood 2000) or triaxial (Mazzei, Curir, 2001; Athanassoula, Misiriotis, 2002; Sellwood 1999) N-Body haloes. Bar instability in stellar disks can be classically inhibited if the galaxy has

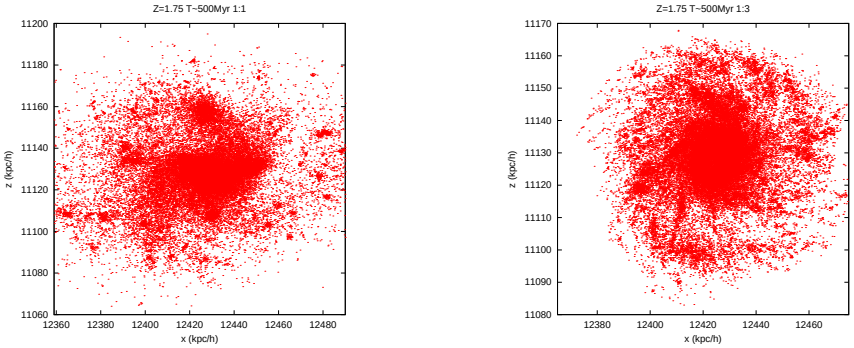

Fig. 5. Stellar disks for cases 1/1, 1/3, at redshift $z = 1.75$. Particles are projected in simulation XY plane. Positions are in the simulation reference frame. The DM halo is not shown.

a spherical halo and the halo mass inside the disk radius is comparable to or greater than the disk mass (Ostriker, Peebles 1973; Efstathiou et al. 1982; Christodoulou et al. 1995). This result has been confirmed by N-Body simulation; however, more recently a possible role of the halo in the opposite effect, namely in enhancing the bar formation has been explored (Curir, Mazzei 1999, Athanassoula 2001) ,suggesting that the debate on the dynamical feedback between dark and baryonic matter if far from being exhausted.

Here we present preliminary results of a new numerical study concerning the growth of bar instability in stellar disks embedded in a fully cosmological halo. We use the parallel tree–code GADGET to follow the gravitational evolution of the two collisionless component, halo and disk, in a cosmological context.

3.1. Setup and parameters of the simulation

We choose a ΛCDM cosmology (same parameters as in simulations C,D) and $25h^{-1}$ Mpc of box size. The halo was selected from a low-resolution run (128^3 particles), it doesn't suffer major mergers since $z = 3$ and it lives in a low-density environment. We re-simulate the halo at 8 times higher resolution, following the whole simulation box with the multi-mass technique described above (Section 1) to account for the large-scale tidal forces. We run five different simulations of the disk+halo system. All of them do use the whole simulation box, employing the resimulation technique to enhance resolution not only in the disk+halo region, but also in a large zone around it, having a size of $\approx 4h^{-1}$ comoving Mpc at $z = 2$, with $\approx 10^6$ high resolution DM particles. This is done to follow accurately the hierarchical evolution of the halo and its accreting satellites and to avoid the presence of any low–mass DM particle, at any z. The mass of high–resolution DM particles is $1.2 \cdot 10^6 h^{-1} M_\odot$. At $z = 0$ the halo has $M \approx 10^{11} h^{-1} M_\odot$ ($\approx 10^5$ particles), $r_v = 97h^{-1}$ kpc and $r_c = 115h^{-1}$ kpc (see Section 2).

We vary two parameters: the stellar to DM mass ratio and the redshift of disk immersion, $z = 2$ and $z = 1$. The evolution of the system spans more than 10 Gyr and more than 7 Gyr down to $z = 0$, respectively. We define the mass ratios (including those quoted for the experiments starting at $z = 1$) using the mass of the halo inside a sphere of radius $r_s = 3r_d$, where $r_d = 20h^{-1}$ *physical* kpc, at $z = 2$. The disk is generated with an exponential density profile, in gravitational equilibrium with the potential of the DM halo, in a plane perpendicular to the angular momen-

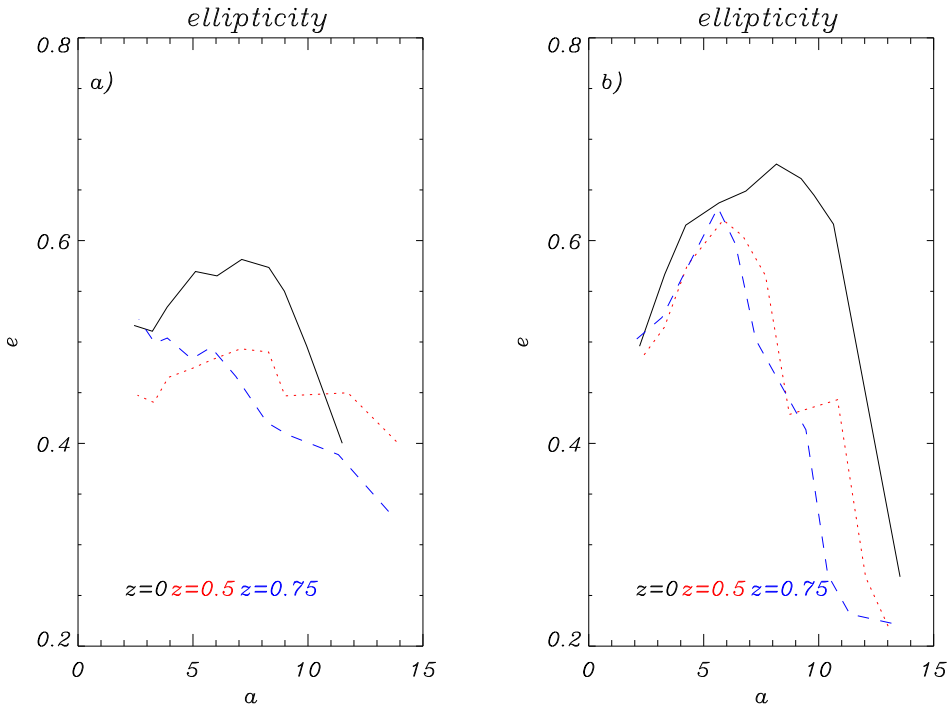

Fig. 6. Behaviours of the ellipticity $1 - b/a$ as function of the semimajor bar axis a (h^{-1} physical kpc) in cases 1/1 (panel a) and 1/3 (panel b) evaluated on density contour levels at three different redshifts. Solid lines correspond to redshift $z = 0$, dotted lines to $z = 0.5$, and dashed lines to $z = 0.75$.

tum of the halo, with a Toomre parameter $Q = 1.5$. We embed it in the cosmological simulation at the selected redshift, so that its center of mass coincides with the position of the minimum of the gravitational potential of the halo, and the bulk velocity of the halo is added to each star particle.

The disk has $5.6 \cdot 10^4$ particles. Our halo sphere has the same number of particle at $z = 2$. We choose as mass ratios M_d/M_h (M_d being the disk mass): 1/1 ($z = 2$ only), 1/3, 1/10. This choice of mass ratios allows us to compare our findings with results for non-cosmological disk+halo systems, provided by previous works (Curir & Mazzei 1999, Mazzei & Curir 2001). In Figure 5, we show the disk after ≈ 500 Myr of evolution for the mass ratios 1/1 and 1/3 and initial redshift $z = 2$. The different evolution for the two mass ratios is evident. In the 1/1 case, the disk is very irregular and fragmented, as it is expected since this mass ratio corresponds to an instability. In the 1/3 case the disk is much more regular, and spiral arms are also sketched.

3.2. Bar instability

Here, we present our preliminary results on the ellipticity of the bar for mass ratios 1/1 and 1/3, when the disk is embedded at a redshift $z = 2$. We estimated the bar feature from the isodensity contour calculated inside the disk. In the 1/1 case the bar forms at $z = 1.85$ and it lasts until z=0. The initial bar is not longer than 6 (physical) kpc, but its length increases with the evolution, extending to more than 10

kpc after z=1. This behaviour is qualitatively consistent with the results of Curir & Mazzei (1999), which show the formation of a long lasting ($\approx$ 1.7 Gyr) bar in disk+halo systems, provided that the halo is still far from relaxation.

The 1/1 case shows the formation of a bar with self similar shapes in the inner density contours. This property is described by the evolution of ellipticity as a function of the semimajor bar axis (Fig. 6). In the 1/3 case the initial bar instability generates a short bar at z=1.7 (approximately $5h^{-1}$ physical kpc). The bar increases its length more slowly than in the 1/1 case, producing a longer and stronger bar in the final state. In the 1/3 case the ellipticity rises to a maximum corresponding to a semimajor axis value ranging between 5 and 8 h^{-1} kpc, and then drops. Assuming $b/a = 0.6$ as the threshold value to define a strong bar (Mazzei and Curir 2001), and defining the *bar length* as the value of a corresponding to $b/a = 0.4$, we see that the final (at $z = 0$) length of the bar is $\approx 11h^{-1}$ kpc in the case 1/1 and $\approx 13h^{-1}$ kpc in the case 1:3.

We will use our full set of simulations to investigate the impact of the cosmological environment on topics directly related to the bar instability, which have recently raised an interesting and somewhat controversial debate: among the others, the angular momentum transfer between the star and DM component (Weinberg& Katz 2002; Valenzuela & Klypin 2002; El-Zant & Shlosman 2002), the role of the cosmological haloes in triggering or suppressing the bar instability (Athanassoula 2001), the stability of the bar feature (Curir & Mazzei 1999) and the heating of the stellar disk (Velasquez & White 1999; Navarro 2001).

Acknowledgements. We thank INAF for allowing us the CPU time to perform the ART simulation C and D at the CINECA consortium (grant cnami44a on the SGI Origin 3800 machine), and part of the GADGET simulation of the stellar disk+DM halo simulations (grant cnato43a, inato003 on the IBM SP3/SP4 machine). GADGET simulations of high–resolution clusters and part of the stellar disk+DM halo simulations have been run on the 16 Linux PC Beowulf cluster at the Osservatorio Astronomico di Torino. Alessandro Gardini is thanked for allowing us to make use of the simulations A and B; we also wish to thank him, Loris Colombo, Giuseppe Tormen, Elena D'Onghia, Andreas Burkert for useful discussions about the different topics presented here.

References

Athanassoula, E. , astro-ph/0112077, 2001
Athanassoula, E., Bosma, A., Papaioannou, S. 1987, A&A, 179, 23
Athanassoula, E., Misirotis, A., 2002, MNRAS, 330,35
Brian, G. & Norman, M., 1998, ApJ, 495, 80
Bullock, J.S., Kolatt, T.S., Sigad, Y., Somerville, R.S., Kravtsov, A.V., Klypin, A.A., Primack, J.R., & Dekel, A., 2001, MNRAS, 321, 559
Christodoulou, D. M., Shlosman, I., Tohline, J. E., 1995, ApJ, 443, 551
Curir, A. & Mazzei,P., 1999, A&A, 352, 103
Debattista, V. P., Sellwood, J. A. 2000, ApJ, 543, 704
de Blok, McGaugh, S.S., & Rubin, V.C., W.J.G., AJ, 2001, 122, 2396
Efstathiou, G., Lake G., Negroponte, J., 1982, MNRAS, 199, 1069
Eke, V.R., Cole, S., & Frenk, C.S., 1996, MNRAS, 282, 263
Eke, V., Navarro, J. & Frenk, C., 1998, ApJ, 503, 569E
El-Zant, A., Shlosman, I., 2002, astro-ph/0203390
Gardini, A., Murante, G. & Bonometto, S. A., 1999, ApJ, 524, 510
Gott, R. & Rees, M. 1975, A&A, 45, 365G
Katz, N., & White, S.D.M., 1993, ApJ, 412, 455
Kravtsov A., Klypin A. & Khokhlov A., 1997 ApJ, 111, 73 K
Lahav, O., Liljc, P. R., Primack, J. R. & Rees, M., 1991, MNRAS, 282, 263E

Macciò A. V., Gardini A., Ghigna S. & Bonometto S. A., 2002, ApJ, 564, 1M
Macció, A.V., Murante, G., & Bonometto, S., 2003, Apj, accepted
Mazzei, P. & Curir, A. 2001, A&A, 372, 803
Navarro, J.F., 2001, astro-ph/0110681
Navarro, J.F., Frenk, C.S., & White, S.D.M., 1996, ApJ, 462, 563
Navarro, J.F., Frenk, C.S., & White, S.D.M., 1997, ApJ, 490, 493
Ostriker J. P., Peebles P. J. E., Ap.J., 186, 467 , 1973
Sellwood, J. A., 1981, A&A, 99, 36
Sellwood, J.A., in "Astrophysical disks", Sellwood & Goodman editors, ASP Conf. Series 160, p. 327 (1999)
Springel V., Yoshida N. & White S.D.M., 2001 NewA, 6, 79 S
Tormen, G., Bouchet, F., & White, S.D.M., 1997, MNRAS, 286, 865.
van den Bosch, F.C., & Swaters, R.A., 2001, MNRAS, 325, 1017
Valenzuela, O., Klypin, A., 2002, astro-ph/0204028
Velaszquez, H., White, S.D.M., 1999, MNRAS, 304,254
Weinberg, D.M., Katz, N., 2991, astro-ph/0110632